

# Design of 3D-printed Foot Interface for Operating Multiple Monitors in a Surgical Robot System

Myoungjae Jun,<sup>1</sup> Choonsung Shin,<sup>2</sup> and Hieyong Jeong<sup>1\*</sup>

<sup>1</sup>Department of Artificial Intelligence Convergence, Chonnam National University,  
77 Yongbong-ro, Bukgu, Gwangju 61186, Republic of Korea

<sup>2</sup>Graduate School of Culture, Chonnam National University,  
77 Yongbong-ro, Bukgu, Gwangju 61186, Republic of Korea

(Received August 24, 2023; accepted September 19, 2023)

**Keywords:** foot interface, 3D printing technology, web-based platform, operating multiple monitors, surgical robot, embedded system

Owing to the effect of the Coronavirus disease (COVID-19) pandemic, the use of surgical robots to reduce the risk of infection to medical staff has been gradually increasing. In surgeries involving a surgical robot, the surgeon adjusts the robot's arms and camera by operating an input interface with their hands and/or feet. However, owing to the diverse types of input information required for surgery, the necessity to match the operation between input information and the input interface is increasing. Thus, we propose a foot interface based on three-dimension (3D)-printer technology and verify its usefulness through a demonstration. First, the current level and direction of development of foot interfaces are reviewed through a detailed assessment of the foot interfaces used in surgical robots. Then, the hardware platform for the proposed interface is designed and fabricated using a 3D printer, and the necessary electronic systems are embedded in the hardware platform. Finally, the usefulness of this interface is demonstrated. In terms of the appropriateness of expanding the input function through the foot interface, similarities and differences in some tasks are discussed by conducting an experiment in which the same task as that of the hand interface is performed using the proposed foot interface. In addition, the ability to improve the usage of the foot interface through training is discussed.

## 1. Introduction

The use of surgical robots is expected to increase gradually as the capabilities of robots to perform various types of surgery grow.<sup>(1)</sup> Moreover, the risk of infection to medical staff, such as Coronavirus disease (COVID-19) infection, has accelerated the use of surgical robots.<sup>(2)</sup> In robotic surgery, a doctor sits behind a console that provides a high-resolution three-dimensional view and uses the console to remotely manipulate two robotic arms inserted into the patient's body.<sup>(3)</sup> Because the surgeon's hands should be fixed on the surgical tools during the operation, the assistance of a surgical assistant is required.<sup>(4,5)</sup> For example, a camera assistant must coordinate well with a doctor. However, if the operation time is prolonged and the assistant is

\*Corresponding author: e-mail: [h.jeong@jnu.ac.kr](mailto:h.jeong@jnu.ac.kr)  
<https://doi.org/10.18494/SAM4625>

fatigued by performing repetitive actions, resulting in hand tremors, unstable images may be obtained, which may hamper the operation.<sup>(6)</sup>

A camera-locking system can be used as an alternative to this issue. After setting the desired camera view, a surgeon can use the console to perform surgery. However, if the surgeon must change the current camera view during a surgery, they must first release the current surgical instrument and then unlock the camera-locking system. Thereafter, the surgeon must set the appropriate camera view, lock it again, pick up the instruments, and resume the surgery. The additional process of regulating the camera angle distracts the surgeon from the surgical procedure, which requires high concentration. Therefore, other alternatives for changing the camera view, such as head direction control,<sup>(7–9)</sup> voice control,<sup>(10)</sup> finger control,<sup>(11,12)</sup> pneumatic control,<sup>(13)</sup> gaze control,<sup>(14,15)</sup> tongue control,<sup>(16,17)</sup> and foot switch control,<sup>(18,19)</sup> have been proposed.

These alternatives help the surgeon to focus with both hands on the console during surgery, but they may be limited to specific purposes. Head direction control can distract the surgeon, who must be able to coordinate full-body movements using their sightline and head.<sup>(7–9)</sup> Voice recognition may fail because of ambient noise or the voice instructions of other medical staff, and the available command vocabulary may be limited.<sup>(10)</sup> In addition, because the surgeon must communicate frequently with the surgical assistant during a surgery, the robot would need to determine whether the doctor's voice is meant to change the camera view or communicate with the surgical assistant. Finger control is not hands-free, and therefore, it can affect the surgery depending on the surgeon's unintended hand gestures.<sup>(14,15)</sup> EMARO, an endoscope manipulator robot, is the pneumatically driven endoscopic holder robot that can operate flexibly and smoothly with the use of air pressure.<sup>(13)</sup> These examples highlight the necessity and limitations of hands-free interfaces for the problem of setting the camera view. In addition to setting the camera view, the collection of various types of information and the support of auxiliary devices are needed so that the surgeon can collect information and understand the results accurately during surgery.

In a recent study, an interface that allows a surgeon to control a surgical robot by using their feet and hands was proposed,<sup>(18,19)</sup> and its effectiveness and potential during surgery were reported. However, many problems associated with the precise control of a surgical robot through the surgeon's feet need to be solved. Unlike a hand-operated mouse, the foot pedal currently used to control surgical robots is limited to the simple function of a button click. Therefore, in this study, we aim to design a 3D-printed foot interface that can realize multiple functions. A prototype in which four monitors display images of the surgeon zooming in and out on the selected target in an image by using the designed foot interface is developed to verify the interface's effectiveness.

## 2. Related Works

Table 1 shows the related studies classified on the basis of the measurement parameter. Depending on the sensing parameter, the category can be divided into three primary parameters: methods to implement functions with pedals as the sensor, with pressing force, and with foot position. Detailed descriptions of each main sensing parameter are provided in the following

Table 1  
Related studies classified on the basis of measurement parameter.

| Category | Author                                   | Sensing parameter                              | Sensor type           |                           |
|----------|--|--|-----------------------|---------------------------|
| Force    | J. Gillbert <sup>(20)</sup>              | Binary switch                                  | Pedal                 |                           |
|          | B. Paul Moraviec <sup>(21)</sup>         |  | Pedal                 |                           |
|          | Schurr <i>et al.</i> <sup>(22)</sup>     |  | Pedal                 |                           |
|          | R. Thorlakson <sup>(23)</sup>            |  | Pedal                 |                           |
|          | Metzler and Hall <sup>(24)</sup>         |  | Pedal                 |                           |
|          | Mora <sup>(25)</sup>                     |  | Pedal                 |                           |
|          | J. Elkins <sup>(26)</sup>                |  | Pedal                 |                           |
|          | Goldberg <i>et al.</i> <sup>(27)</sup>   |  | Pedal                 |                           |
|          | M. Munro <sup>(28)</sup>                 |  | Pedal                 |                           |
|          | Minor <i>et al.</i> <sup>(29)</sup>      |  | Pedal                 |                           |
|          | Voros <i>et al.</i> <sup>(30)</sup>      |  | Pedal                 |                           |
|          | MTGH100 <sup>(31)</sup>                  |  | Pedal                 |                           |
|          | Mirbagheri <i>et al.</i> <sup>(32)</sup> |  | Pedal                 |                           |
|          | Wang <i>et al.</i> <sup>(34)</sup>       |  | Continuous force      | Switches and transducers  |
|          | Abdi <i>et al.</i> <sup>(18,19)</sup>    |  |                       | Pistons and foot rotation |
| Position | E. Abdi <sup>(35)</sup>                  | Foot patterns                                  | Pressure sensor sheet |                           |
|          | Chen <i>et al.</i> <sup>(36)</sup>       | Position switch                                | IMU sensor            |                           |
|          | Dai <i>et al.</i> <sup>(37)</sup>        | Separate each DOF                              | IMU sensor            |                           |
|          | Abdi and Olivier <sup>(38)</sup>         | Translational and rotational movements of foot | Mechanical components |                           |

subsections. None of the existing foot interfaces implements all functions with clicks (left/right), drag, and scroll (zoom in/out), unlike hand interfaces.

## 2.1 Pedal interface

The button interface is the most common type of foot pedal interface. It usually consists of several binary switches/buttons; one switch can perform two functions: on/off. For example, EndoAssist<sup>(20)</sup> and FreeHand,<sup>(21)</sup> which use head tracking to control the robot, are equipped with simple foot switches to prevent unintended movements. These prevention mechanisms allow for movement only while the surgeon is pedaling. Likewise, the Trocar and Instrument Positioning System Karlsruhe (TISKA)<sup>(22)</sup> has a pedal that can lock or unlock tool movement. Additionally, foot pedals have been developed to control microscopes in microsurgery,<sup>(23)</sup> activate tools in ophthalmic surgery,<sup>(24)</sup> control drill tool speeds in dental procedures,<sup>(25)</sup> and control prosthetic arms.<sup>(26)</sup>

The da Vinci system<sup>(27)</sup> uses two types of foot pedal. These pedals are used to activate the camera or change the robotic arm rather than directly control it. In the S system, released in 2006, all buttons were on a flat platform. However, the Si system, released in 2009, had a modified arrangement with several pedals that moved either up, down, or perpendicular to the sidewall.

In robotic surgery, a pedal interface can be used to control endoscope movement. When the pedal is pressed, the speed of the slave tool must be constant. For example, the Endex endoscopic positioning system developed by Andronic Device Ltd.<sup>(28)</sup> features a single-degree-of-freedom

(DoF) motion. The two-footed pedal allows the surgeon to insert and withdraw the scope through the trocar. Postural Mechatronic Assistance Solo Surgery (PMASS)<sup>(29)</sup> is a wearable endoscope introduced in 2009, and it can control the upward and downward movements of an endoscope with three DoFs.

In Vision Kontrol endoscopy (ViKY)<sup>(30)</sup> a robotic endoscope holder system developed by Endocontrol Medical Company, a pedal interface is used to control the robot with three DoFs. The MTGH100 endoscope holder developed by HIWIN Technologies Corp.<sup>(31)</sup> features a six-way control pedal. The surgeon can operate the endoscope by using the pedal along six directions (in, out, up, down, left, and right).

The RoboLens endoscope holder robot<sup>(32,33)</sup> uses two types of pedal interface. The first type of interface is equipped with a switch with two pedals. The right pedal is used to control the camera's lateral movement (up, down, left, and right), and the left pedal is used to zoom in and out of images. In the second type of interface, which is wearable, a pedal with an optical sensor responds to movements of both feet. Surgeons can control the left, right, forward, and backward endoscope movements with the right foot and the forward and the backward endoscope movements with the left foot.

## 2.2 Force-based foot interface

The force with which a pedal is pressed can be used to provide continuous input to a robot. For example, the surgical robot AESOP<sup>(34)</sup> has a foot interface, and it was experimentally confirmed that the speed to press the pedal was linearly related to foot force. The surgeon can move the endoscope in, out, left, right, up, or down by applying pressure to the corresponding button on the foot interface. This interface replaced the voice-based camera control interface in the AESOP 2000 system.<sup>(10)</sup> An elastic isometric foot interface<sup>(35)</sup> was developed to control robotic endoscope holders. This interface allows for continuous control along three DoFs by pressing six pistons, and a fourth DoF is provided by the rotation of one foot about a vertical axis. Because the spring force is sensed using a Hall-effect proximity sensor, the control range is limited. Accordingly, the slave robot can only move at a constant speed when forces greater than 3 N are applied.

## 2.3 Foot interface based on position

Although foot movements are not as precise as hand movements, positional information can be used as control commands. To control endoscope motion, foot rotation information can be collected using an inertial measurement unit (IMU) sensor attached to the foot.<sup>(36)</sup> When the rotation angle of the foot exceeds a predetermined threshold, robot joint motion is activated. With the similar design using IMU attached to operator's foot, each DOF needs to be activated separately and cannot be combined, although the interface can control joints' movements of robot in four DOFs.<sup>(37)</sup>

An interface with a structure in which two linear guides and two rotary joints were connected in series from the base to the pedal<sup>(38)</sup> was conceived. Each joint collected positional information about one DoF of the foot. A magnetic membrane potentiometer tracked the translational motion

of the interface, and an encoder tracked its rotational motion. A disadvantage of this control strategy was the limited working space of the controlled device. The operational accuracy of the slave part might not be guaranteed because of foot motion errors. Moreover, the selected tandem structure can increase the overall height of the foot interface and cause the coupling of foot motions.

### 3. System Design

#### 3.1 Hardware design

In this study, we propose a foot interface, as shown in Fig. 1. The horizontal length is 180 mm, the vertical length is 194 mm, and the depth is 14 mm. The proposed foot interface recognizes clicks on a plate and dragging motions. On the basis of these functions, it can serve as an external input device that takes cues from the feet. The hardware configuration required to implement the foot interface is considered. Figure 1 presents an isometric view of the designed foot interface, which shows the 3D-printed and embedded systems, including two microcontrollers and various types of sensor. The types and arrangement of electronic components inside the device can be seen in this figure. Inside a platform that is of the same size as a general human body weighing scale, force sensors are placed at each corner to measure the intensity of applied force. The load cell used in weight scales is used as the force sensor. This load cell can measure a maximum weight of 50 kg, and four load cells are installed at each corner. It has a response speed of 10 ms. A load cell and button are used to sense the pressure of the interface. The load cell has a resolution of 24 bits and can hold a maximum weight of 50 kg. The button is composed of a component that can withstand a weight of 100 kg. Figure 2 shows a 3D design drawing of the foot interface, which was used to assemble the 3D-printed materials. All parts required for the assembly were 3D-printed, and the necessary electronic parts and two

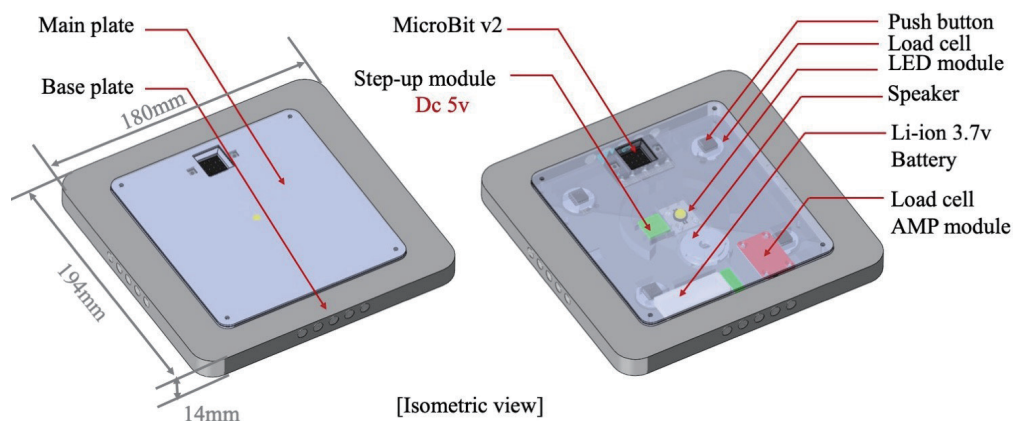
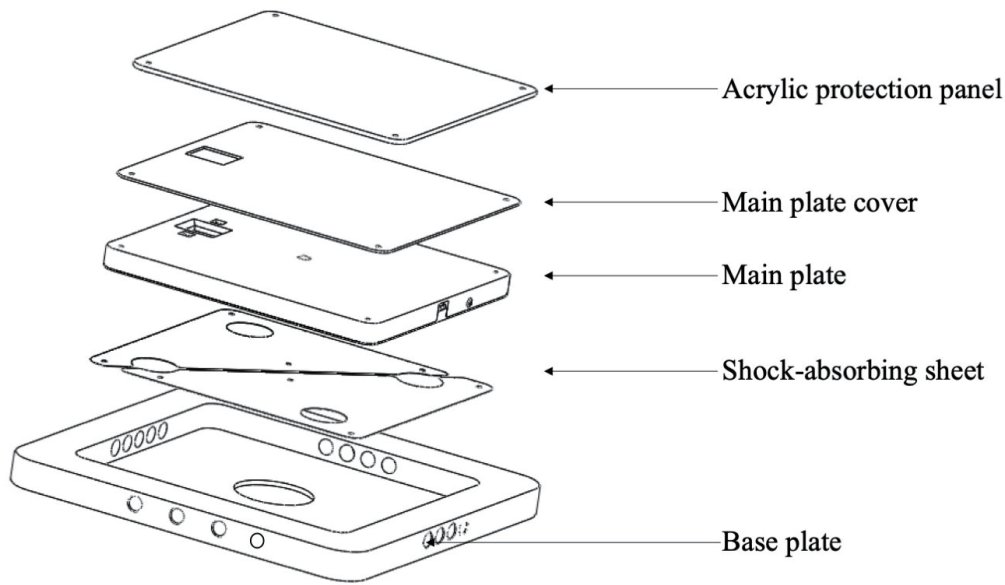


Fig. 1. (Color online) Isometric view of designed foot interface: 3D-printed and embedded systems, including two microcontrollers and various types of sensor.



[Assembly drawing]

Fig. 2. 3D design drawing of foot interface for assembling 3D-printed materials.

microcontrollers used herein, namely, Arduino and Micro:Bit, were placed in the assembly. It is okay if a user moves feet less than 20 m/s because the device size is less than 200 mm and the response speed is 10 ms. Because the operating environment does not need to move quickly, the specification can perform the function of an interface.

The signal obtained from the force sensor is converted into a digital value by the microcontroller's analog-to-digital converter (ADC). Then, the average value of the four force sensors is calculated and used in real time by the moving average filter. When a force is applied by considering the arrangement of individual sensors, the measured values of the four force sensors can be used to identify the corner of the platform in which the produced force is concentrated. When  $p_i$  ( $i = 1, 2, 3, 4$ ) corresponds to the four sensors, the measured values are expressed as a ratio of  $W_B$  by setting the user's body weight ( $W_B$ ) to 1. The values are used to recognize pressing and dragging forces on the surface. This can be expressed as<sup>(36)</sup>

$$\begin{aligned}
 GRF_{p_1} &= \frac{p_1}{W_B} \times 100(\%), \\
 GRF_{p_2} &= \frac{p_2}{W_B} \times 100(\%), \\
 GRF_{p_3} &= \frac{p_3}{W_B} \times 100(\%), \\
 GRF_{p_4} &= \frac{p_4}{W_B} \times 100(\%).
 \end{aligned}
 \tag{1}$$

Here,  $W_B$  represents the participant's weight.  $W_B$  can be obtained as  $W_B = p_1 + p_2 + p_3 + p_4$  (kg) by standing on the developed foot interface. In addition, to recognize dragging, it is necessary to measure the position of the center of pressure (CoP). A change in position can be determined using Eq. (2).<sup>(37–42)</sup>

$$x_{CoP} = \frac{\sum_{i=1}^4 (p_i \times x_i)}{\sum_{i=1}^4 p_i} \text{ (mm)}$$

$$y_{CoP} = \frac{\sum_{i=1}^4 (p_i \times y_i)}{\sum_{i=1}^4 p_i} \text{ (mm)}$$
(2)

Here,  $(x_i, y_i)$  are the coordinates indicating the position of the load cell. When the original position is set as the center coordinates  $(0, 0)$ , the position coordinates of each load cell can be calculated.

An IMU sensor is installed at the center of the hardware platform. Acceleration is measured in terms of the impacts along the  $x$ -,  $y$ -, and  $z$ -axes when a force is applied to the surface of the platform. The impact pattern of the platform can be identified when the acceleration information of each sensor is acquired and analyzed against a pretrained threshold. Because this information allows for the precise analysis of the foot force produced on the surface, various patterns can be generated. These patterns can be used in the medical interface to control various systems utilized in the operating room by matching them to keys on a keyboard. In addition, by recognizing the starting location of the foot interface as the coordinates of the origin, it is possible to prevent malfunctions by recognizing cases in which the interface location is moved unintentionally and suddenly. Speakers, LEDs, and dot matrices are used to allow the user to check the platform's mode conversion and internal operation. Figure 3 shows the developed foot interface: top (left side) and bottom (right side) views.

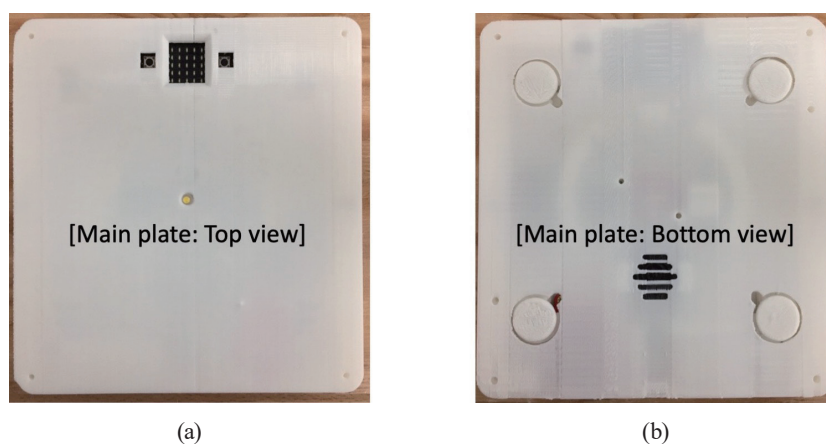


Fig. 3. (Color online) Developed foot interface: (a) top and (b) bottom views.

### 3.2 Embedded system design

The developed platform uses a 3.7-volt rechargeable lithium-ion battery and a USB charging method to recharge the battery. The four force sensors used herein are load cells used in general digital scales. A load cell amplifier (AMP) is configured using the HX711 AMP board with 24-bit resolution. Because the data values of the four load cells must be processed independently, four HX711 AMP boards are prepared. Load cell data, which correspond to button pushes, and IMU data are collected by the Arduino Pro Micro microcontroller (8-bit). The collected data are transmitted to the Micro:Bit controller (32-bit) through UART communication, which then communicates with external devices that control communication, sensing, dot matrix, LED, and speaker output. Figure 4 shows the actual embedded system, electronic parts of the system, and the circuit diagram. Table 2 shows the hardware specifications of the electronic components used to fabricate the foot interface.

### 3.3 Software design

It is necessary to execute three pieces of software to operate the foot interface. The first is the embedded software driven by Arduino to receive analog sensor values from the foot sensors and

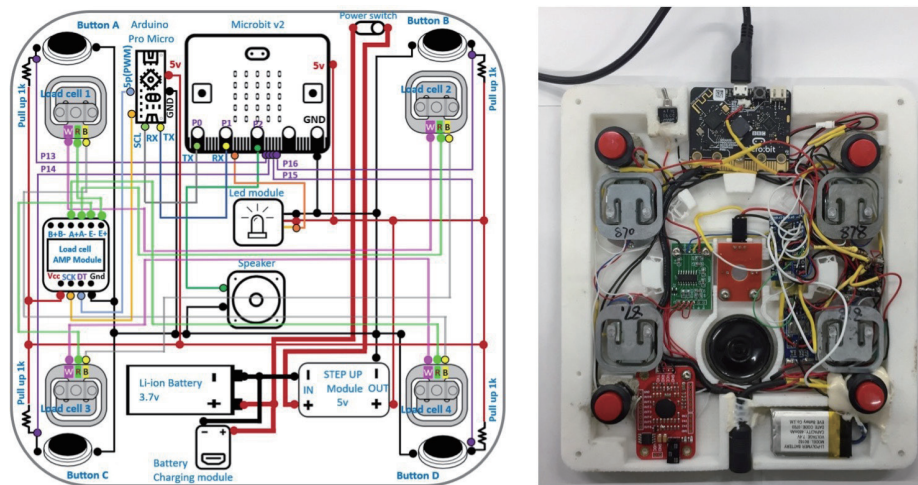


Fig. 4. (Color online) Circuit diagram, electronic parts of system, and actual embedded system.

Table 2  
Hardware specifications of electronic components used to manufacture the foot interface.

| Electric part       | Specification                         |
|---------------------|---------------------------------------|
| Microcontroller     | Micro:Bit ver2 (ARM cortex-M4 32 bit) |
| Operating voltage   | DC 5 V                                |
| Display             | 5 × 5 Dot Matrix (Micro:Bit)          |
| Speaker             | 32Ω, 87 db                            |
| Button              | Push button × 4                       |
| Load cell amplifier | HX711 24-bit resolution               |
| Load cell           | 50 kg (Generic) × 4                   |
| Battery             | 3.7 V Li-ion (3.7 A)                  |

convert them to digital signals through the ADC. The second is for Micro:Bit to recognize and process user input patterns after analyzing the sensor values. Micro:Bit is programmed using micro-Python. The third is a platform based on web programming to operate the foot interface for controlling the information displayed on an external monitor.

Sensor data are bundled into one packet by Arduino and transmitted to Micro:Bit through UART communication at 10 ms intervals. Micro:Bit then analyzes the sensor values to recognize the user's input pattern and transmits the keyboard fundamental values that match the input pattern to the computer. Simultaneously, Micro:Bit controls the input values obtained from the sensors, the  $5 \times 5$  dot matrix including LEDs, and the buzzer included in the interface.

The web-based platform is programmed in Java, and the Eclipse web server is installed and operated on the computer to run as the local server. To use the platform, first, a web browser must be opened, and the address of the local server must be entered into the browser's address bar. When the web page of the monitor screen is opened and the start button is clicked, the foot interface starts to transmit data packets to the computer through UART communication. In the computer, data packets are saved as data.txt files in the local server at 10 ms intervals, and these data.txt files are loaded into the platform and displayed on the external monitor. Figure 5 presents a flowchart depicting the roles of the two microcontrollers: Arduino and Micro:Bit.

Figure 6 shows a flowchart depicting the role of the web-based platform. When the web-based program is executed, the data.txt file is loaded from the local server, and the designed graphic-based console screen is displayed on the web browser screen. The images in the web

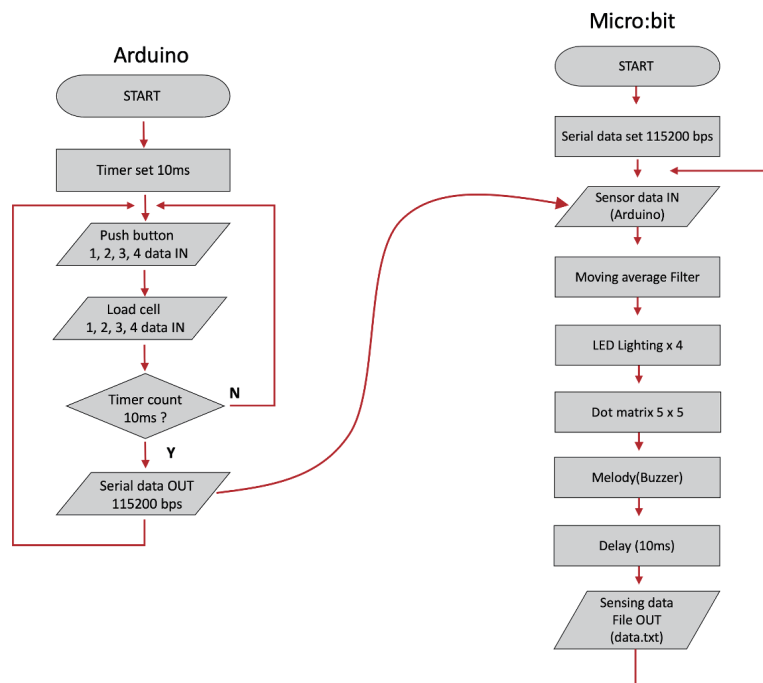


Fig. 5. (Color online) Flowchart showing the roles of the two microcontrollers: Arduino receives sensor values from the foot sensors and converts the sensor values to digital signals through the ADC, and Micro:Bit recognizes and processes user input patterns after analyzing the sensor values.

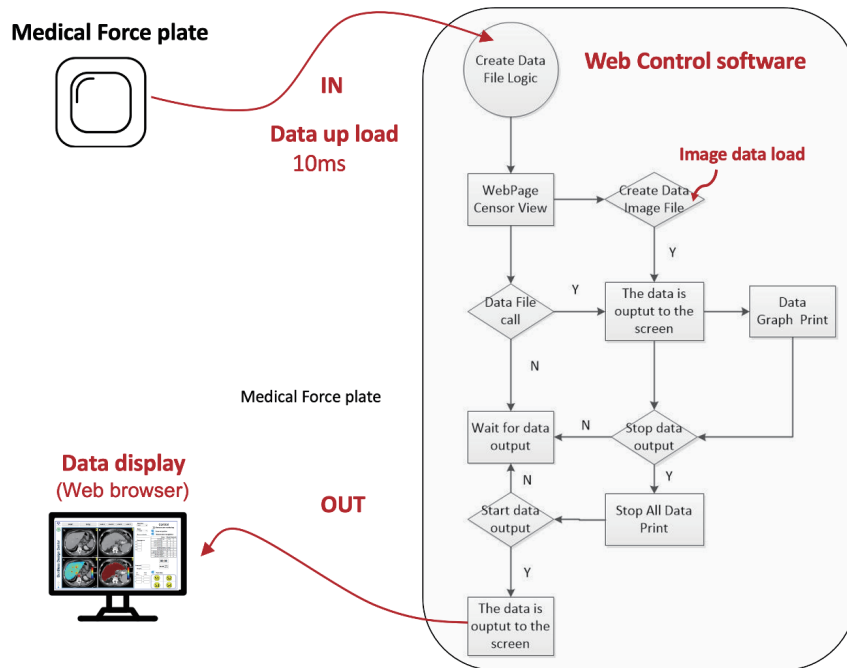


Fig. 6. (Color online) Flowchart showing the role of the web-based platform.

platform are loaded by pressing each load button for loading four medical images A–D. The developed web software provides two modes. One mode handles medical image data, and the other mode checks the data received from the interface in real time. If the start button is clicked after selecting the mode, the received data are reflected in real time and displayed on the console screen. The images on the console screen can be regulated on the basis of the pattern of the foot interface.

## 4. Results

### 4.1 Results of web-based platform

Figure 7 shows the results of the foot interface when the user presses the button to demonstrate the primary function. In mode A, the image already saved in folder A is displayed on the monitor as soon as the user presses it. The S1 button at the bottom right turns orange simultaneously, and the user can see the force and acceleration data changing.

Figures 8 and 9 show screenshots of the web-based platform for manipulating medical images, which was developed to validate the foot interface. The developed web-based platform has two modes. Mode A shows four types of medical image, and the user can select one type of medical image or all four types depending on their needs. When one image type is selected, it is possible to zoom in and out while adjusting the scale of the selected image. In Mode B, time-series data of the four load cells and the three-axis acceleration sensor built into the foot interface



Mode A

Mode B

Fig. 7. (Color online) Results of the foot interface when the user presses the button to demonstrate the basic function.

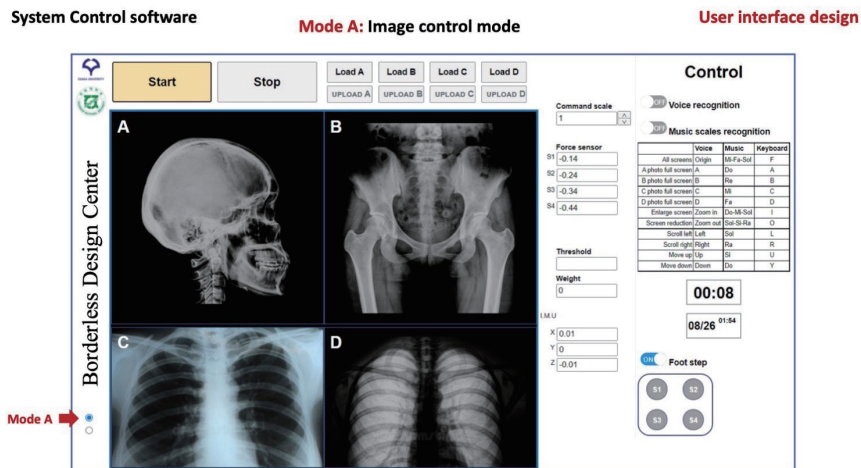


Fig. 8. (Color online) Example of mode A to allow the user to upload and zoom in and out of medical images.

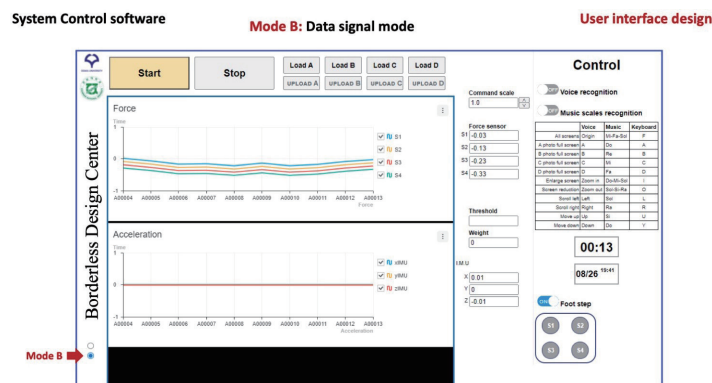


Fig. 9. (Color online) Example of mode B to set the measurement values of the four load cells and the threshold value for determining the click.

can be checked. This mode allows the user to check the operation of the sensor from the developer's perspective, and it is unlikely to be of significant use from the user's perspective.

Developers can make fine adjustments while viewing time-series data when adjusting the degree of click and double-click force, which can lead to differences depending on the user. A load cell and button are used to sense the pressure of the interface. The load cell has a resolution of 24 bits and can hold a maximum weight of 50 kg. The Measurable button is composed of a button that can withstand a weight of 100 kg. The two-axis acceleration sensor value representing the plane is used to determine the malfunction when the click, double-click, or drag event occurs while the interface device is moving owing to the user's malfunction in the foot interface. The value of the acceleration sensor in the direction of gravity is used to receive and determine the values of the load cell and acceleration sensor when a click or double-click is identified.

Table 3 shows foot interface control using the keyboard or foot patterns. The user can control the screen through each button pattern, and each control command is matched with the keyboard keys of the computer so that the user can use the keyboard and the foot interface together. When the user wants to view monitor A in full screen mode among the four monitors, the user clicks the S1 button once (top left corner of the developed system). When monitor A is in the full screen mode, the user can double-click the S2 button (upper right corner of the developed system) to zoom in. The user can double-click the S3 button (lower left corner of the developed system) to zoom out.

In mode A, which is mainly used, a menu in the upper part allows the user to upload multiple medical images and check them simultaneously. Recently, in an increasing number of cases, medical doctors are required to operate while simultaneously checking medical images showing different types of data or viewpoints when performing a surgery. For example, we present a case in which an operation is performed while simultaneously checking CT and MRI image results

Table 3  
Foot interface control with keyboard or foot patterns.

| Function   | Keyboard | Foot pattern |
|--|----------|--------------|
| Display all images                                   | FF       | S1 + S2      |
| Screen A full size                                   | A        | S1           |
| Screen B full size                                   | B        | S2           |
| Screen C full size                                   | C        | S3           |
| Screen D full size                                   | D        | S4           |
| Zoom in  | I        | S2 + S2      |
| Zoom out   | O        | S3 + S3      |
| Move the screen to the left                          | L        | S2 + S4      |
| Move the screen to the right                         | R        | S1 + S3      |
| Move the screen up                                   | U        | S1 + S2      |
| Move the screen down                                 | D        | S3 + S4      |
| IMU, force, Graph Output                             | IF       | S1 + S1      |
| S1 sensor value Graph Output                         | S1       | S1           |
| S2 sensor value Graph Output                         | S2       | S2           |
| S3 sensor value Graph Output                         | S3       | S3           |
| S4 sensor value Graph Output                         | S4       | S4           |
| IMU <i>x, y, z</i> -axis acceleration output         | IM       | S2 + S2      |
| IMU <i>x, y, z</i> -axis angular acceleration output | IMA      | S3 + S3      |

and an endoscope image during surgery. The developed platform simultaneously displays X-ray images of the head, bust, and pelvis, and MRI images of the chest. The scale of the currently visible image is displayed on the right side of the image, and it indicates the scale of zoom-in or zoom-out.

Below that, mode B can be used to set the measurement value of the four load cells and the threshold value for determining a click. In addition, a voice recognition menu is included in the platform. However, it is not included in the experimental results of this study because we believe that it is not practically necessary during surgery. The operation of the proposed foot interface by the keyboard is provided in the platform so that it is possible. Figure 10 shows the test results of the implementation of zoom-in and zoom-out functions after the continuous capturing and selection of video images. Detailed video results are available at the link (<https://youtu.be/2LFaTfuQUw>). Although images in four monitors are operated by hand in the demo, rapid selection among four types of image and zoom-in and zoom-out can be performed using the developed foot interface.



Fig. 10. (Color online) Results of testing the implementation of zoom-in and zoom-out after continuously capturing and selecting video images.

## 4.2 Performance results

Figure 11 shows the system operation to capture part of an image to verify the performance of the foot interface. Figure 11(a) shows different body parts with four uploaded medical images. In Fig. 11(b), when the surface of the interface is clicked by the user's foot, the LED emits light, and the selected image among the four images is displayed. Figure 11(c) shows that an image selected from a different image among the four monitors is displayed. Figure 10(d) shows the results of executing the zoom-in function on the selected monitor through keyboard operation. The user can check the performance of the developed foot interface in detail by visiting the following video link (<https://youtu.be/9xSQCrtMIImo>).

## 5. Discussion

As the need for foot interfaces increases, many studies have reported interface devices that offer the function of clicking a simple button or pedal as an external input device to control a surgical robot. In this study, a foot interface was developed on the basis of 3D printing technology and validated experimentally. Although the number of buttons for providing external inputs to the surgical robot system has increased in this interface, the possibility of using those buttons as input devices raises a few questions.

First, we check whether there were differences when the same task was performed using the hand and foot interfaces separately. In an experiment where the same task was performed using the hand and foot interfaces, it was confirmed that the task time of the foot interface was consistent with that of the hand interface according to Fitts' law and the Steering law. It was confirmed that the task time of the foot interface was longer because target selection using the foot was more arduous than that using the hand. This was because visual feedback could be



Fig. 11. (Color online) Photographs of the process of capturing part of an image to verify the performance of the foot interface.

utilized actively with the hand interface<sup>(43)</sup>. However, in the case of the foot interface, the required time was longer because visual feedback could not be utilized depending on the type and posture of the experiment. However, because it was efficient to perform the steering task with the foot, the task time remained unchanged, even when the difficulty of the task increased. This experimental result confirmed that although the foot interface had clear limitations, it led to marginal differences on some tasks depending on the type of task. Moreover, the results indicated the scope for improving operability by changing the design of the foot interface by considering the type of task.

Then, we examined whether the user's ability to operate the foot interface improved through practice. A word processing task was performed to compare the performance of the user who manipulated the foot interface with that of the user who manipulated the hand interface. The results before and after practice were compared. Although they tried several exercises, additional practice was needed to become more familiar with the device, and they compared the improvements in their task performance. Although the performance of the hand interface could not be confirmed, we confirmed that the user's ability to operate the foot interface improved significantly through practice.<sup>(44)</sup> This indicates the potential of the foot interface, suggesting that with enough practice, users could use the foot interface as an external input device for word-processing tasks.

Through the above discussion, the advantages and disadvantages of the foot interface were briefly summarized, and it could be inferred that various types of design research attempt were needed to determine which design was better to improve the operability of the foot interface according to the task at hand.

## 6. Conclusion

Human–computer interfaces for operating surgical robots were reviewed. In particular, with a focus on foot interfaces, it was found that the existing foot interfaces were composed mainly of switches, pedals, and buttons, which limited the input to a maximum of three-degree-of-freedom motion. These foot interfaces provided limited discrete velocity and direction, and their disadvantages included lack of feedback information through haptic devices. When such a foot interface is used, the user must visually check the foot's posture frequently, which increases the complexity of control and, possibly, the user's fatigue. Therefore, we developed a new foot interface by using 3D printing technology so that a trackpad, a type of hand interface that is familiar to users, can be used as a foot interface, and we verified its performance through a demonstration.

## Acknowledgments

This research was supported by the “Technology Commercialization Collaboration Platform” program of the Korea Innovation Cluster (Project Number: 2022-DD-RD-0065) and by a National Research Foundation of Korea (NRF) grant funded by the Korea Government (MSIT) (No. 2021R1F1A1047682).

## References

- 1 C. D'Ettorre, A. Mariani, A. Stilli, F. Baena, P. Valdastris, A. Deguet, P. Kazanzides, R. Taylor, G. Fischer, S. DziMaio, A. Mencias, and D. Stoyanov: *IEEE Rob. Autom. Mag.* **28** (2021) 56. <https://doi.org/10.1109/MRA.2021.3101646>
- 2 C. Fleming, A. Fullard, S. Croghan, G. Pellino, and F. Pata: *J. Clin. Med.* **11** (2022) 2957. <https://doi.org/10.3390/jcm11112957>
- 3 G. Yang, J. Cambias, K. Cleary, E. Daimler, J. Drake, P. Dupont, N. Hata, P. Kazanzides, S. Martel, R. Patel, V. Santos, and R. Taylor: *Sci. Rob.* **2** (2017) eaam8638. <https://doi.org/10.1126/scirobotics.aam863>
- 4 M. Nurok, T. Sundt, and A. Frankel: *Anesthesiol Clin.* **29** (2011). 1. <https://doi.org/10.1016/j.anclin.2010.11.012>
- 5 L. Lingard, R. Reznick, S. Espin, G. Regehr, and I. DeVito: *Acad. Med.* **77** (2002) 232. <https://doi.org/10.1097/00001888-200203000-00013>
- 6 H. Mohrmann-Lendla and A. Fleischer: *Ergonomics* **34** (1991) 353. <https://doi.org/10.1080/00140139108967319>
- 7 S. Kommu, P. Rimington, C. Anderson, and A. Rane: *J. Rob. Surg.* **1** (2007) 133. <https://doi.org/10.1007/s11701-007-0010-5>
- 8 J. Stolzenburg, T. Franz, P. Kallidonis, D. Minh, A. Dietel, J. Hicks, M. Nicolaus, A. Ai-Aown, and E. Liatsikos: *BJU Int.* **107** (2011) 970. <https://doi.org/10.1111/j.1464-410X.2010.09656.x>
- 9 K. Tadano and K. Kawashima: *Int. J. Med. Rob. Comput. Assisted Surg.* **11** (2015) 331. <https://doi.org/10.1002/rcs.1606>
- 10 Y. Wang and D. Uecker: USA Patent No. US6463361B1 (2002). <https://patents.google.com/patent/US6463361B1/en> (Accessed 6 August 2023).
- 11 R. Polet and J. Donnez: *Surg. Technol. Int.* **17** (2008) 187.
- 12 G. Buess, A. Arezzo, M. Schurr, F. Ulmer, H. Fisher, L. Gumb, T. Testa, and C. Nobman: *FIPS Endoarm Surg. Endosc.* **14** (2000) 395. <https://doi.org/10.1007/s004640020066>
- 13 D. Yoshida, S. Maruyama, I. Takahashi, A. Matsukuma, and S. Kohnoe: *Asian J. Endosc. Surg.* **13** (2020) 448. <https://doi.org/10.1111/ases.12760>
- 14 D. Noonan, G. Mylonas, J. Shang, C. Payne, A. Darzi, and G. Yang: 2010 3rd IEEE RAS & EMBS Int. Conf. Biomed. Rob. Biomechatron. (2010). <https://doi.org/10.1109/BIOROB.2010.5628078>
- 15 C. Staub, S. Can, B. Jensen, A. Knoll, and S. Kohlbecher: 2012 4th IEEE RAS & EMBS Int. Conf. Biomed. Rob. Biomechatron. (2012). <https://doi.org/10.1109/BioRob.2012.6290850>
- 16 L. Andreasen Struijk: *IEEE Trans. Biomed. Eng.* **53** (2006) 2594. <https://doi.org/10.1109/TBME.2006.880871>
- 17 D. Johansen, C. Cipriani, D. Popovic, and L. Struijk: *IEEE Trans. Biomed. Eng.* **63** (2016) 1368. <https://doi.org/10.1109/TBME.2016.2517742>
- 18 E. Abdi, E. Burdet, M. Bouri, S. Himidan, and H. Bleuler: *Sci. Rep.* **6** (2016) 21758. <https://doi.org/10.1038/srep21758>
- 19 E. Abdi, E. Burdet, M. Bouri, and H. Bleuler: *PLoS One* **10** (2015) e0134501. <https://doi.org/10.1371/journal.pone.0134501>
- 20 J. Gilbert: *Ann. R. Coll. Surg. Engl.* **91** (2009) 389. <https://doi.org/10.1308/003588409X392162>
- 21 P. Moraviec: USA Patent No. US9639953B2 (2017). <https://patents.google.com/patent/US9639953> (Accessed 6 August 2023).
- 22 M. Schurr, A. Arezzo, B. Neisius, H. Rininsland, H. Hilzinger, J. Dorn, K. Roth, and G. Buess: *Surg. Endosc.* **13** (1999) 528. <https://doi.org/10.1007/s004649901029>
- 23 R. Thorlakson: USA Patent No. US5787760A (1998). <https://patents.google.com/patent/US5787760> (Accessed 6 August 2023).
- 24 M. Metzler and M. Hall: USA Patent No. US6689975B2 (2004). <https://patents.google.com/patent/US6689975>. (Accessed 6 August 2023).
- 25 A. Mora: USA Patent No. US8076599B2 (2009). <https://patents.google.com/patent/US8076599B2/en> (Accessed 6 August 2023).
- 26 J. Elkins: USA Patent No. US20040078091A1 (2007). <https://patents.google.com/patent/US20040078091> (Accessed 6 August 2023).
- 27 R. Goldberg, M. Hanuschik, H. Hazebrouck, P. Millman, D. Kapoor, J. Zabinski, D. Robinson, D. Weir, and S. Brogna: USA Patent No. US8120301B2 (2012). <https://patents.google.com/patent/US8120301B2/en> (Accessed 6 August 2023).
- 28 M. Munro: *J. Am. Assoc. Gynecol. Laparosc.* **1** (1993) 67. [https://doi.org/10.1016/s1074-3804\(05\)80763-7](https://doi.org/10.1016/s1074-3804(05)80763-7)
- 29 A. Minor, R. Ordorica, J. Villalobos J, and M. Galan: *Ann. Biomed. Eng.* **37** (2009) 643. <https://doi.org/10.1007/s10439-008-9626-5>

- 30 S. Voros, G. Haber, J. Menudet, J. Long, and P. Cinquin: IEEE/ASME Trans. Mechatron. **15** (2010) 879. <https://doi.org/10.1109/TMECH.2010.2080683>
- 31 HIWIN website: <https://pdf.medicaexpo.com/pdf/hiwin-technologies/hiwin-robotic-endoscope-holder/123582-230246.html> (Accessed 6 August 2023).
- 32 A. Mirbagheri, F. Farahmand, A. Meghdari, and F. Karimian: RoboLens. Scientia Iranica **18** (2011) 105. <https://doi.org/10.1016/j.scient.2011.03.012>
- 33 A. Mirbagheri, F. Farahmand, B. Ghanadi, K. Khoiy, S. Porsa, M. Shamsollahi, M. Owlia, F. Karimian, and K. Toulabi: Front. Biomed. Technol. **2** (2015) 184.
- 34 Y. Wang, K. Laby, D. Uecker, A. Mangaser, and M. Ghodoussi: USA Patent No. US5878193A (1999). <https://patents.google.com/patent/US5878193A/en> (Accessed 6 August 2023).
- 35 E. Abdi: EPFL Thesis (2017). <https://doi.org/10.5075/epfl-thesis-7343>
- 36 J. Chen, I. Leung, D. Navarro-Alarcon, W. Lin, P. Li, D. Lee, Y. Liu, and M. Tong: Laryngoscope **126** (2016) 566. <https://doi.org/10.1002/lary.25634>
- 37 X. Dai, B. Zhao, Y. He, Y. Sun, and Y. Hu: Front. Biomed. Devices (2017) DMD2017-3421. <https://doi.org/10.1115/DMD2017-3421>.
- 38 E. Abdi, M. Bouri, J. Olivier, H. Bleuler: 2016 4th Int. Conf. Rob. Mechatron. (ICROM) (2016). <https://doi.org/10.1109/ICRoM.2016.7886826>
- 39 H. Jeong, K. Yamada, M. Kido, S. Okada, T. Nomura, and Y. Ohno: IEEE J. Transl. Eng. Health Med. **4** (2016) 2100311. <https://doi.org/10.1109/JTEHM.2016.2599185>
- 40 H. Jeong and Y. Ohno: Intell. Serv. Rob. **10** (2017) 323. <https://doi.org/10.1007/s11370-017-0227-8>
- 41 H. Jeong, M. Kido, and Y. Ohno: 2016 38th Ann. Int. Conf. IEEE Eng. Med. Biol. Soc. (EMBC) (2016) 4573. <https://doi.org/10.1109/EMBC.2016.7591745>
- 42 T. Wang, H. Jeong, and Y. Ohno: IEEE Access **5** (2017) 17816. <https://doi.org/10.1109/ACCESS.2017.2747841>
- 43 T. Wang, H. Jeong, M. Watanabe, Y. Iwatani, and Y. Ohno: Mech. Syst. Signal Process. **113** (2018) 90. <https://doi.org/10.1016/j.ymssp.2017.01.051>
- 44 S. Hong and S. Kim: J. Ergonomics Soc. Korea **31** (2012) 725 (in Korean).
- 45 F. Garcia and K. Vu: Comput. Human Behav. **27** (2011) 285. <https://doi.org/10.1016/j.chb.2010.08.006>

## About the Authors



**Myoungjae Jun** received his Ph.D. degree in mechatronics engineering from Hanyang University, south korea, in 2018. From 2010 to 2018, he was a student researcher(full-time) with Korea Institute of Industrial Technology. From 2019 to 2021, he was an special researcher (full-time) with the Department of Robotics & Design for Innovative Healthcare, Graduate School of Medicine, Osaka University, Suita, Japan. Since 2022, he has been working as an associate postdoctoral researcher (full-time) with the Department of Artificial Intelligence Convergence, Chonnam National University, Republic of Korea. His research interests include Biomimetics robot platform, Underwater robot, and Embedded system. ([21cnehemiah@gmail.com](mailto:21cnehemiah@gmail.com))



**Choonsung Shin** received his B.S. degree in Computer Science from Soongsil University in 2004. He received his M.S. and Ph.D. degrees in Information and Communication (Computer Science and Engineering) from the Gwangju Institute of Science and Technology (GIST), in 2006 and 2010, respectively. He was a Postdoctoral Fellow at the HCI Institute of Carnegie Mellon University (CMU) from 2010 to 2012. He was a principal researcher at Korea Electronics Technology Institute (KETI) from 2013 to 2019 and a CT R&D Program Director of Ministry of Culture, Sports and Tourism (MCST) from 2018 to 2019. In September 2019, he joined the Graduate School of Culture, Chonnam National University where he is currently an associate professor. His research interests include culture technology & contents, VR/AR and Human-Computer Interaction. ([cshin@jnu.ac.kr](mailto:cshin@jnu.ac.kr))



**Hieyong Jeong** received his Ph.D. degree in mechanical engineering from Osaka University, Japan, in 2009. From 2009 to 2013, he was a senior research engineer (full-time) with Samsung Heavy Industries, Company, Ltd., Daejeon, Republic of Korea. From 2013 to 2014, he was a researcher (full-time) with Chonnam National University, Gwangju, South Korea. From 2014 to 2019, he was an associate professor (full-time) with the Department of Robotics & Design for Innovative Healthcare, Graduate School of Medicine, Osaka University, Suita, Japan. Since 2019, he has been working as an associate professor (full-time) with the Department of Artificial Intelligence Convergence, Chonnam National University, Republic of Korea. His research interests include robotic intelligence, and artificial intelligence of things (AIoT) system. ([h.jeong@jnu.ac.kr](mailto:h.jeong@jnu.ac.kr))